2

Capacity Improvement for Densely Deployed Small Cell Networks

As one of the key requirements in the 5G mobile communications system, the capacity improvement technology by using densely deployed small cell networks is considered as an efficient solution. In this chapter, both problems and challenges of the capacity improvement technology are introduced in detail. Then, three typical frequency allocation schemes, such as orthogonal frequency allocation, co-channel frequency allocation, hybrid frequency allocation, are proposed by using the capacity analysis with theoretical proofs in the densely deployed small cell networks scenario. The optimal geographic region division scheme is also proposed for small cell networks with closed-form solutions. At last, the self-deployment procedure of hybrid frequency allocation scheme is designed and the performances of proposed schemes are verified by numerous results in this chapter.

2.1 Introduction of Problems and Challenges

According to recent studies, 50% of phone calls and 70% of data services will take place indoors for the coming years [1]. Moreover, about two thirds voice services and 90% of data services will take place indoors [2]. Studies also show that more than 45% of households and 30% of businesses users' experienced inadequate indoor coverage in [3], leading to the poor quality of service (QoS). Furthermore, Cisco forecasts that the global mobile data traffic grows by 81% in 2013 and smarter mobile devices are increasing fast in [4]. Moreover, the traffic demands are surging rapidly for the 5G wireless networks. But the uneven traffic distribution leads to new challenges for the capacity improvement. The traditional network planning and optimization techniques can not guarantee a wide range wireless network coverage and an effective service quality indoors, leading to the expansion of network capacity as a fundamental problem for 5G wireless networks.

Furthermore, traditional capacity improvement techniques such as cell splitting and employing more spectrum resources can not meet the unexpected surging capacity demands, uneven traffic distribution in geography and time domains, and various service requirements. Besides, due to the building block, shadow effect, signal propagation loss, and reflection effect, the capacity holes in hotspots and deteriorated user experiences are new challenges [5]. Therefore, how to make full use of heterogeneous network resources, how to decrease the complexity of resource management, and how to improve the network capacity and the user experience indoors are still big problems unsolved. Traditional network planning and optimization techniques face the problems of high implementation cost, long deployment period, and complex optimization process. Therefore, the self-optimization of densely deployed small cells, such as femtocell, picocell, and microcell, are proposed and considered as an efficient solution in [6]-[7] for the capacity and coverage enhancements indoors.

As one of the efficient capacity enhancement techniques, small cells are introduced to operate on licensed bands for both indoor and outdoor scenarios in [3] and [8]. Furthermore, small cells can provide a fast, flexible and cost-efficient solution for existing cellular networks in [9], which include femtocells, picocells, microcells and metrocells [10]. Also, small cells can be deployed in hotspots and indoor scenarios to improve the network capacity and user's experience. However, the challenges for densely deployed small cells still exist, including the interference management, frequency allocation, and access mode selection schemes for small cells in 5G wireless networks.

In the literature, existing research works on capacity improvement by using small cells are studied in terms of different frequency allocation schemes and interference management issues. For the uplink capacity analysis in hierarchical networks, both the closed subscriber group (CSG) access and open access modes are considered in orthogonal frequency division multiple access (OFDMA) and

time division multiple access (TDMA) based femtocell networks in [8]. Besides, the macrocell users' density is considered as a key factor for the optimal CSG and open access modes selection where the open access mode is much preferred when macrocell users' density is small. Moreover, the open access mode is applied in code division multiple access (CDMA) based femtocell networks in [11]. And a distributed orthogonal frequency allocation scheme is proposed by using the optimal frequency allocation ratio between femtocell and macrocell networks in [12] to minimize the interference among different layers in hierarchical networks. In [13], both the joint and disjoint sub-channel allocation schemes are proposed for two-tier networks with quality of service constraints in terms of success transmission probabilities and per-tier minimum rates. Considering the frequency allocation in hierarchical networks, a hybrid orthogonal frequency allocation scheme is proposed in [14], which considers about the distance between femtocell and macrocell and the interference constraint area (ILCA) factor.

In terms of the interference problems among OFDMA based hierarchical networks, a realtime multi-agent reinforce learning technology based intelligent self-organized femtocell network is proposed in [15] by using the accumulated interference from different femtocell networks to solve these problems. Moreover, a docition based realtime scheme is proposed in [15] to improve the learning ability and accuracy of Q-learning process, which solves the unstable decision making problem and the drawbacks of complex learning process with a slow learning speed. Considering the uplink capacity and interference cancelation problems in CDMA based hierarchical networks, the uplink capacity and time hop based TH-CDMA interference cancelation technology are proposed and analyzed with the outage probability constraints of macrocell and femtocell in a co-channel frequency deployment scenario [16]. Furthermore, in OFDMA based hierarchical networks, self-configuration and self-optimization based

interference cancelation schemes are proposed to solve the interference problems in co-channel and orthogonal frequency allocation schemes in [17]-[18].

Considering the scarcity of spectrum resources, the small cell sharing the same spectrum with macrocells is an efficient way to increase the network capacity. Recent study works on the frequency allocation and capacity analysis for small cells are using co-channel and orthogonal frequency allocation schemes in a single cell scenario, which apply the interference cancelation methods to improve the network capacity. However, considering that small cells are typically deployed randomly by users without network planning, it is important that the intelligent self-organizing techniques should be applied in small cells. Besides, more and more researchers are paying much attention to adding cognitive technologies in femtocell networks in [19]-[21]. But how to add intelligent abilities for small cells optimization is a new challenge. Therefore, a hybrid frequency allocation scheme is proposed in this chapter to increase the downlink capacity in the scenario of densely deployed small cell networks. First, the downlink network capacity of small cell networks is analyzed by using different frequency allocation schemes, including orthogonal, co-channel, and hybrid frequency allocation schemes. Both the density of small cells and interference constraints to guarantee the quality of macrocells are considered and verified with theoretical results in this chapter. The proposed hybrid frequency allocation scheme utilizes different frequency allocation schemes for the inner and outer circle regions to improve the network capacity. By adding the geographic region cognition ability in densely deployed small cells, an optimal geographic region division scheme is designed and the optimal square zone length is theoretically obtained for an efficient information delivery among small cells via cognitive pilot channel (CPC) [22]-[23]. Numerical results verify that the proposed novel schemes can improve the network capacity in [29] by using appropriate small cells deployments.

2.2 Capacity Analysis Using Different Frequency Allocation Schemes

2.2.1 System Model and Scenario

A typical architecture of heterogeneous networks is depicted in Figure 2.1 with overlapped macrocell base stations (MBSs) and small cells. Three different frequency allocation schemes, including orthogonal, co-channel, and hybrid frequency allocation schemes, are described and compared in this section, considering the impacts on downlink capacity and interference in heterogeneous networks.

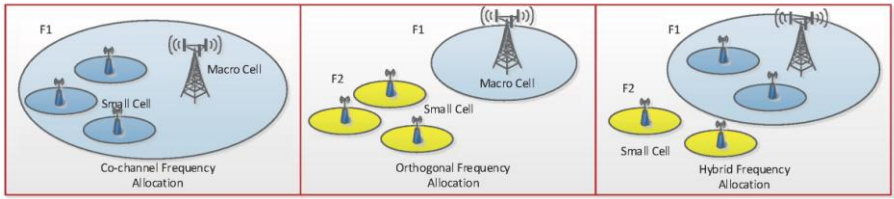

Figure 2.1 *Small cell network architecture and three frequency allocation schemes. SOURCE: Reproduced with permission from [29]. Copyright 2015 Springer International Publishing.*

(1) Orthogonal Frequency Allocation: Different frequency bands are assigned to macrocell layer and small cell layer separately. Although the orthogonal frequency allocation can reduce cross-layer interference, it has a disadvantage of lower spectral efficiency. Furthermore, due to the scarce of available spectrum, the intra-cell interference among small cells is a big problem, especially in the densely deployed small cell scenario.

(2) Co-channel Frequency Allocation: Both macrocell and small cell share the same frequency. Due to its low transmit power and small coverage area, the inter-cell interference between macrocell and small cell can be avoided by using the spatial isolation scheme, which can improve the network capacity. However,

when the small cells are densely deployed, the interference issues can not be solved only by using the spatial isolation scheme.

(3) Hybrid Frequency Allocation: The coverage area of macrocell is divided into inner and outer circle regions. Small cells located within the inner circle region apply the orthogonal frequency allocation scheme, in order to decrease the interference to macrocell. When small cells are located in the outer circle region, the co-channel frequency allocation scheme can be applied to improve the network capacity by utilizing the spatial isolation scheme to minimize the interference.

It is also assumed that the coverage area of MBS is modeled as a hexagon with radius R_m, and the coverage area is represented by H as $|H| = 3\sqrt{3}R_m^2$. The distribution of macrocell user equipment (MUE) is a Poisson Point Process (PPP) [24]-[26] with the density λ_{MUE}. The position of MUE is depicted as $\Phi_{MUE} = \{X_i\}$. Each MBS has six neighbors denoted by MBS_i (i=1, 2... 6). The distribution of small cells, such as femto base station (FBS) is modeled as a PPP [24]-[26] with the density λ_{FBS}. The position of FBS is represented as $\Phi_{FBS} = \{Y_i\}$. The OFDMA-based LTE system is used and no power control scheme is applied in the downlink. Thus, MBS transmission power is depicted by P_m and FBS transmission power is depicted by P_f. To guarantee the quality of signal in heterogeneous networks in terms of the outage probability ε, the SINR (Signal to Interference plus Noise Ratio) of MUE and femtocell user equipment (FUE) located at the cell edge should be greater than the target SINR Γ_{target}. The amount of RB is N where MBS occupies N_m and the number of RB that FBS occupied depends on different frequency allocation schemes used by FBS. For example, in the orthogonal frequency allocation scheme, $N_f = N - N_m$. When in

the co-channel frequency allocation scheme, $N_f = N_m = N$. $\rho = N_m / N$ denotes the ratio of RB resources that MBS occupies to the overall resources. $\rho = 1$ denotes that the co-channel frequency allocation scheme is used, while $0 < \rho < 1$ is the orthogonal frequency allocation scheme. Considering that the backhaul among MBS and small cells is non-ideal, the information exchange among them faces the challenge of long time delay issues. Therefore, the cognitive pilot channel (CPC) technique [22] is proposed to realize the effective information delivery among MBS and small cells.

2.2.2 Orthogonal Frequency Allocation Scheme

In the orthogonal frequency allocation scheme, different frequency bands are separately assigned to the macrocell and small cell layers, which can decrease the cross-layer interference. As show in Figure 2.2, MUEs located at the edge of MBS_0 using the specific RB resource in the downlink will receive strong interference from the neighbor MBS_i. Given the whole number of RB N and the available RB $N_m = \rho N$, the probability of co-channel interference received by MUE is $1/(\rho N)$. Similarly, the probability of co-channel interference received by FUE from neighbor FBSs is $1/(N - N_m) = 1/[(1-\rho)N]$.

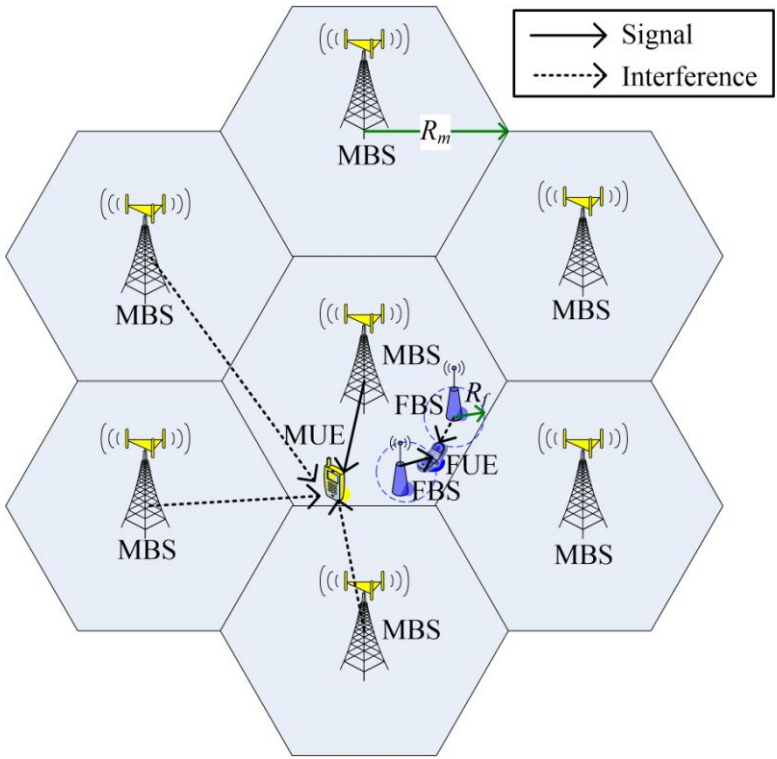

Figure 2.2 *Scenario of orthogonal frequency allocation scheme. SOURCE: Reproduced with permission from [29]. Copyright 2015 Springer International Publishing.*

(1) The SINR of MUE in the downlink is depicted by $SINR_m^{orth}\left(d_m\right)$ in (1).

$$SINR_m^{orth}\left(d_m\right)=\frac{G_m P_m d_m^{-\alpha}}{N_0+\frac{1}{\rho N}\sum_{I=1}^{6} I_{m_i,m}} \tag{1}$$

$$\sum_{I=1}^{6} I_{m_i,m}=\sum_{i=1}^{6} G_{m_i} P_m \bar{d}_{m_i,m}^{-\alpha} \tag{2}$$

G_m is the channel gain which is modeled as a negative exponential distribution with the mean of 1. P_m is the transmit power of MBS, α is the

path loss ratio, N_0 represents the background noise power per RB, d_m is the distance between MBS_0 and MUE, $I_{m_i,m}$ is the co-channel interference to MUE in MBS_0 from MBS_i, $\bar{d}_{m_i,m}$ is the mean distance between neighbour MBS_i and MUE in MBS_0.

To simplify the analysis, it is also assumed that only the strongest interference from MBS_k to MUE is considered, where $\bar{d}_{m_i,m} = R_m$. Then, the coverage radius R_m of MBS satisfies (3) in terms of the maximum outage probability of ε.

$$P(SINR_m^{orth}(R_m) \geq \Gamma_{target}) = \exp\left(-\frac{\Gamma_{target} N_0}{P_m R_m^{-\alpha}}\right)\frac{1}{1+\Gamma_{target}/(\rho N)} \geq 1-\varepsilon \quad (3)$$

$$N_m = \rho N \geq N_{m,\min} = \frac{\Gamma_{target}(1-\varepsilon)}{\exp(-\frac{\Gamma_{target} N_0}{P_m R_m^{-\alpha}}) - (1-\varepsilon)} \quad (4)$$

To guarantee the $SINR_m^{orth}$ quality of MUE with the interrupt probability ε constraints, the number of RB should be higher than $N_{m,\min}$. When the MBS transmit power $P_m = 20\text{W}$, the background noise power $N_0 = 10^{-12}\text{W}$, $\Gamma_{target} = 3$, $\varepsilon = 0.1$, the path loss ratio $\alpha = 4$, the system bandwidth is 20MHz, and the RB resource $N = 110$. Figure 2.3 shows that how the probability of $SINR_m^{orth} > \Gamma_{target}$ changes with ρ and R_m. There is a minimum number of RB resources to guarantee the cell edge MUE's quality. And the minimum number RB increases with R_m. When $R_m = 288\text{m}$, and $\rho = 0.25$, the minimum $N_m = 28$. When $R_m = 500m$, and $\rho = 0.28$, the minimum $N_m = 31$. When $R_m = 800\text{m}$, and $\rho = 0.61$, the minimum $N_m = 68$.

When each MUE occupies one RB resource, the maximum capacity in the downlink is given by (5).

$$C_m^{orth} = \log_2(1+\Gamma_{target}) \tag{5}$$

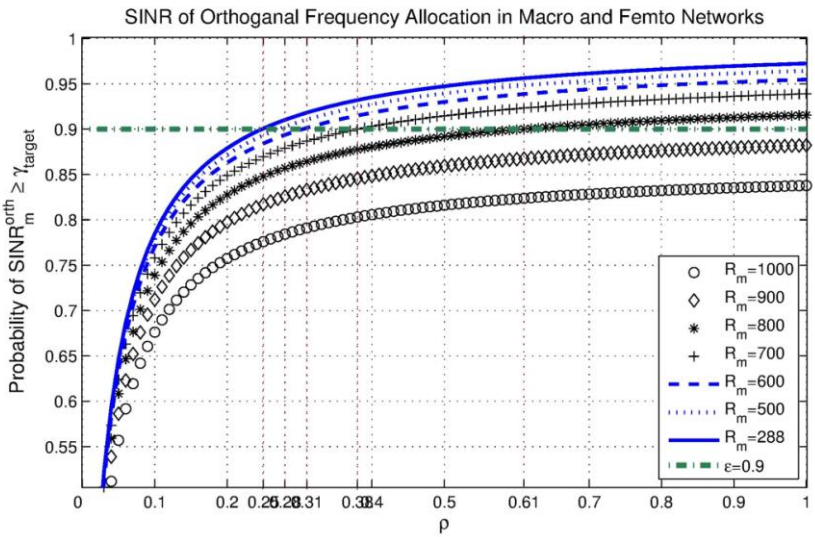

Figure 2.3 *SINR of MUE for different* ρ *and* R_m*. SOURCE: Reproduced with permission from [29]. Copyright 2015 Springer International Publishing.*

(2) The SINR of FUE in the downlink is depicted by $SINR_f^{orth}\left(d_f\right)$ in (6).

$$SINR_f^{orth}(d_f) = \frac{G_f P_f d_f^{-\alpha}}{N_0 + \frac{1}{(1-\rho)N} I_{f,f}} \tag{6}$$

$$I_{f,f} = \sum_{Y_i \in \Phi_{FBS}^P \setminus \{Y_0\}} G_{Y_i} P_f \left\| Y_i \right\|^{-\alpha} \tag{7}$$

G_f is the channel gain which is modeled as a negative exponential distribution with the mean 1. d_f is the distance between FBS and FUE, $I_{f,f}$

denotes the co-channel interference from neighbor FBSs. G_{Y_i} and $\|Y_i\|$ depict the channel gain and the distance between FBS at location Y_i and FUE. And the results in [24] [25] [28] are depicted in (8), where $K_\alpha = 2\pi/[\alpha sin(2\pi/\alpha)]$, and $\hat{\lambda}_{FBS}$ is the maximum density of FBS.

$$\begin{aligned} E[\exp(-sI_{f,f})] &= \exp[-2\pi\hat{\lambda}_{FBS}\int_0^\infty \frac{u}{1+u^\alpha/(sP_f)}du] \\ &= \exp(\hat{\lambda}_{FBS}\, p_f^{2/\alpha} s^{2/\alpha} K_\alpha) \end{aligned} \tag{8}$$

Considering the worst case of the interference from MBS, the SINR of FUE at the cell edge of FBS should be greater than the target SINR threshold Γ_{target} with the outage probability ε in (9).

$$P(SINR_f^{orth}(R_f) \geq \Gamma_{target}) = 1-\varepsilon \tag{9}$$

In the orthogonal frequency allocation scheme, the maximum density of FBS $\hat{\lambda}_{FBS}$ is depicted in (10).

$$\hat{\lambda}_{FBS} = \frac{-\ln(1-\varepsilon) - \frac{\Gamma_{target}}{P_f R_f^{-\alpha}} N_0}{R_f^2 \Gamma_{target}^{2/\alpha} K_\alpha (1-\rho)^{-2/\alpha} N^{-2/\alpha}} \tag{10}$$

Thus, the total system capacity is depicted by C^{orth} in (11).

$$\begin{aligned} C^{orth} &= N_m C_m^{orth} + N_s C_s^{orth} = N[\rho C_m^{orth} + (1-\rho) C_s^{orth}] \\ &= N[\rho + (1-\rho)\hat{\lambda}_{FBS}|H|]\log_2(1+\Gamma_{target}) \end{aligned} \tag{11}$$

The maximum density of FBS $\hat{\lambda}_{FBS}$ is constrained by the resource ratio ρ and the coverage radius of FBS R_f, as shown in Figure 2.4. With a fixed R_f, available RB resources of FBS will decrease with the increase of ρ, where the

interference among different FBS will increase. In order to guarantee the quality of FUE, the density of FBS should decrease to mitigate the interference by utilizing the spatial isolation scheme among FBSs. Moreover, considering the quality of MUE at the cell edge, FBS density achieves the maximum $\hat{\lambda}_{FBS,max}$, when MBS occupies RB resources with the minimum value $\rho_{m,min} = N_{m,min} / N$ and FBS has the maximum value $N_{f,max} = (1-\rho_{m,min})N$. For example, when $R_m = 500\text{m}$, $\rho_{m,min} = 0.28$, the maximum $N_{f,max} = 79$. When $R_f = 10\text{m}$, the maximum density of FBS achieves $\hat{\lambda}_{FBS,max} = 1.10*10^{-3}$. When $R_f = 20\text{m}$, the maximum density of FBS achieves $\hat{\lambda}_{FBS,max} = 2.74*10^{-4}$. Thus, both the RB resource ratio ρ and the coverage radius R_f will affect the maximum density of FBS in the orthogonal frequency allocation scenario.

When each FBS occupies one RB resource, the downlink capacity is given by (12).

$$C_f^{orth} = \hat{\lambda}_{FBS} |H| \log_2(1+\Gamma_{target}) \tag{12}$$

Therefore, when the system bandwidth is N, and the RB resource ratio is $\rho = N_m / N$, the total capacity in the downlink is given by (13).

$$\begin{aligned} C^{orth} &= N_m C_m^{orth} + N_f C_f^{orth} \\ &= N[\rho + (1-\rho)\hat{\lambda}_{FBS} |H|] \log_2(1+\Gamma_{target}) \end{aligned} \tag{13}$$

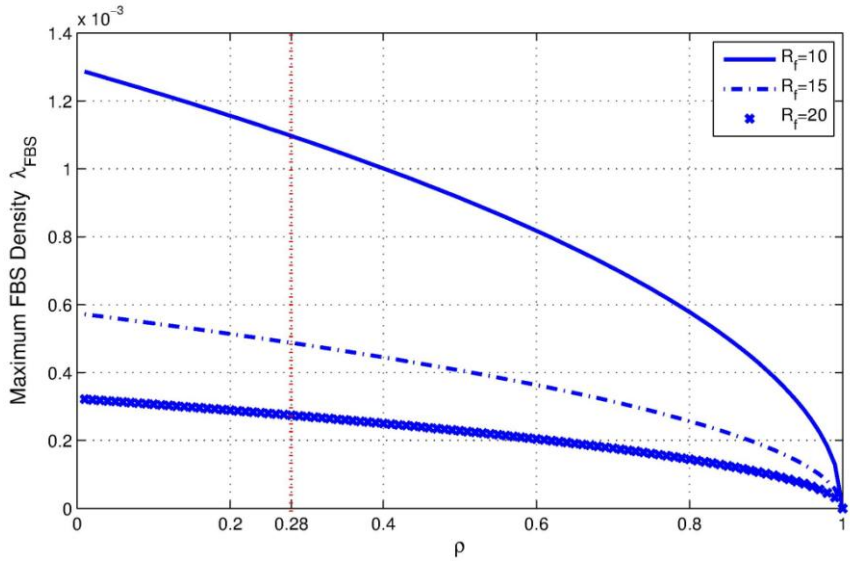

Figure 2.4 *FBS density* $\hat{\lambda}_{FBS}$ *with different* ρ *and* R_f *. SOURCE: Reproduced with permission from [29]. Copyright 2015 Springer International Publishing.*

Furthermore, the maximum total capacity in the downlink is defined as an optimization problem in (14), when the optimal ρ is chosen.

$$\begin{aligned} &\rho^* = \text{argmax}(\text{C}^{\text{orth}}) \\ &s.t.\ N_{m,min} / N \le \rho < 1 \end{aligned} \tag{14}$$

$$\because C^{orth} = A_1[\rho + B_1(1-\rho)^{1+2/\alpha}]$$

$$\therefore dC^{orth} / d\rho = A_1[1 - B_1(1+2/\alpha)(1-\rho)^{2/\alpha}] = 0$$

$$\therefore \rho_{min} = 1 - [\frac{1}{B_1(1+2/\alpha)}]^{\alpha/2} \tag{15}$$

Where $B_1 = |H| N^{2/\alpha}[-\ln(1-\varepsilon) - \Gamma_{\text{target}} N_0 / P_f R_f^{-\alpha}] / (R_f^2 \Gamma_{\text{target}}^{2/\alpha} / K_\alpha)$ and $A_1 = N \log_2(1+\Gamma_{\text{target}}) = 2N$. Therefore, the maximum value C^{orth} is achieved at $\rho = N_{m,min} / N$ in Figure 2.5.

To ensure the quality of MUE and FUE, the total capacity C^{orth} achieves the maximum $C^{orth} = 1.13*10^5$ bit/s when the FBS density is $\hat{\lambda}_{FBS,max} = 1.10*10^{-3}$, where $R_m = 500$m, $\rho \geq \rho_{m,min} = 0.28$, and $R_f = 10$m. When $R_f = 20$m, the total capacity $C^{orth} = 2.83*10^4$ bit/s with the FBS density of $\hat{\lambda}_{FBS,max} = 2.74*10^{-4}$.

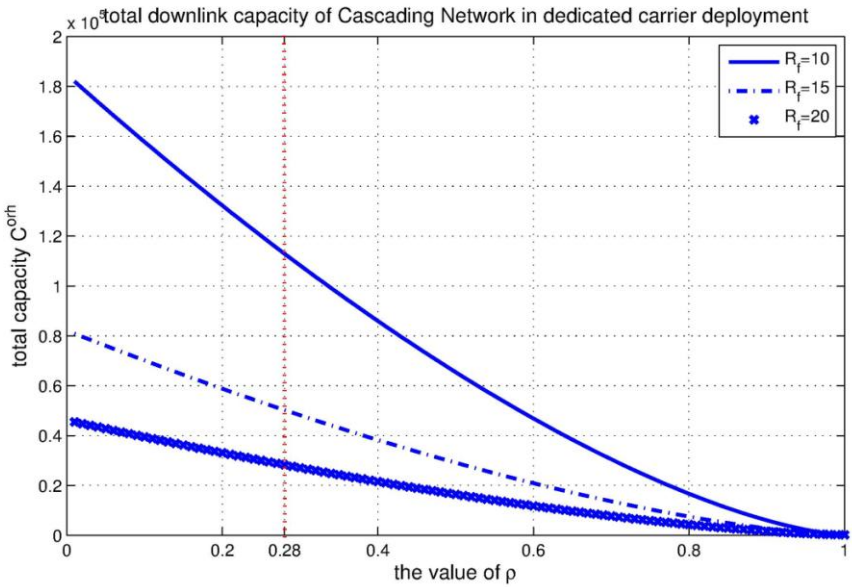

Figure 2.5 *System capacity in orthogonal frequency allocation scheme with different ρ and R_m. SOURCE: Reproduced with permission from [29]. Copyright 2015 Springer International Publishing.*

2.2.3 Co-channel Frequency Allocation Scheme

Although the orthogonal frequency allocation scheme can suppress the co-channel interference among macrocells and small cells, it reduces the spectral efficiency. In terms of the scarce spectrum resources, the co-channel frequency allocation scheme has been paid much attention recently to improve the spectral efficiency. In terms of densely deployed small cells, new types of interference are brought forward, such as the interference from FBS to nearby MUE in the downlink, and neighbour MBS to MUE at the cell edge. Moreover, FUE at the cell edge will suffer the strong co-channel interference from neighbour MBS in the downlink. Therefore, the density of FBS is a key factor that will affect the capacity of hierarchical networks using the co-channel frequency allocation scheme.

Therefore, this section will analyze key influential factors to FBS density and find out the optimal FBS density to improve the downlink capacity of hierarchical networks. Different types of interference are depicted in Figure 2.6. In terms of RB resources of N, the probability of MUE that suffers the co-channel interference from MBS_i is $1/N$. The probability of FUE that sufferers the co-channel interference from neighbour FBSs is $1/N$.

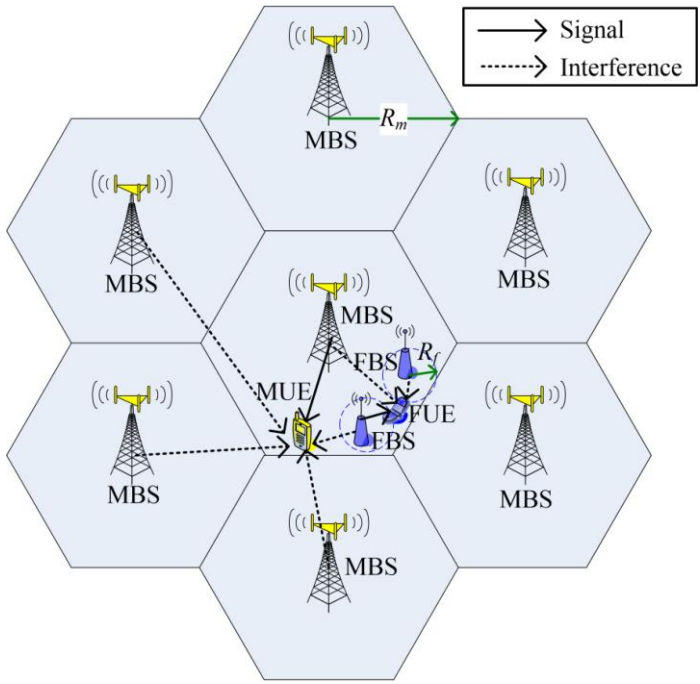

Figure 2.6 *Scenario of co-channel frequency allocation scheme. SOURCE: Reproduced with permission from [29]. Copyright 2015 Springer International Publishing.*

(1) The SINR of MUE in the downlink is depicted by $SINR_m^{coch}\left(d_m\right)$ in (16).

$$SINR_m^{coch}(d_m)=\frac{G_m P_m d_m^{-\alpha}}{N_0+\frac{1}{N}\sum_{i=1}^{6} I_{m_i,m}+\frac{1}{N} I_{f,m}} \tag{16}$$

$$\sum_{i=1}^{6} I_{m_i,m} = \sum_{i=1}^{6} G_{m_i} P_m \bar{d}_{m_i,m}^{-\alpha}$$

$$I_{f,m} = \sum\nolimits_{Y_i \in \Phi_{FBS}^{P}} G_{Y_i} P_s \left\| Y_i \right\|^{-\alpha} \tag{17}$$

$I_{f,m}$ is the co-channel interference from FBS to MUE in MBS_0. $I_{m_i,m}$ is the co-channel interference from neighbour MBS_i to MUE in MBS_0. $\bar{d}_{m_i,m}$ depicts the mean distance for MUEs in MBS_i and MBS_0.

Considering the SINR of MUE at the cell edge with the outage probability constraint ε, $SINR_m^{coch}$ satisfies the constraint in (18).

$$P(SINR_m^{coch}(R_f) \geq \Gamma_{target}) = 1-\varepsilon \tag{18}$$

By applying (16) in (18), the maximum density of FBS $\hat{\lambda}_{FBS,MUE}$ is depicted in (19).

$$\hat{\lambda}_{FBS,MUE} = \frac{-\ln\left[(1-\varepsilon)\left(1+\frac{\Gamma_{target}}{N}\right)\right] - \frac{\Gamma_{target} N_0}{P_m R_m^{-\alpha}}}{N^{-\frac{2}{\alpha}} R_m^2 \left(\frac{P_f \Gamma_{target}}{P_m}\right)^{2/\alpha} K_\alpha} \tag{19}$$

(2) Similarly, the SINR of FUE at the cell edge with the outage probability constraint ε is depicted by $SINR_f^{coch}(d_f)$ in (20).

$$SINR_f^{coch}\left(d_f\right) = \frac{G_f P_f d_f^{-\alpha}}{N_0 + \frac{1}{N} I_{f,f} + \frac{1}{N}\sum_{i=0}^{6} I_{m_i,f}} \tag{20}$$

$$I_{f,f} = \sum_{Y_i \in \Phi_{FBS}^p \setminus \{Y_0\}} G_{Y_i} P_f Y_i^{-\alpha} \tag{21}$$

$$\sum_{i=0}^{6} I_{m_i,f} = \sum_{i=0}^{6} G_{m_i} P_m \bar{d}_{m_i,f}^{-\alpha} \tag{22}$$

$I_{f,f}$ is the co-channel interference from neighbour FBS in the same MBS. $I_{m_i,f}$ is the co-channel interference from neighbour MBS_i. $\bar{d}_{m_i,f}$ depicts the mean distance for FUEs in MBS_i and MBS_0.

Considering the SINR of FUE at the cell edge with the outage probability constraint ε, $SINR_f^{coch}$ satisfies the constraint in (23).

$$P(SINR_f^{coch}(R_f) \geq \Gamma_{target}) = 1-\varepsilon \tag{23}$$

The maximum density of FBS $\hat{\lambda}_{FBS,FUE}$ is depicted in (24).

$$\bar{\lambda}_{FBS,FUE} = \frac{-\ln\left[(1-\varepsilon)\left(1+\frac{\Gamma_{target}P_m R_m^{-\alpha}}{P_f R_f^{-\alpha} N}\right)^2\right] - \frac{\Gamma_{target}N_0}{P_f R_f^{-\alpha}}}{N^{-\frac{2}{\alpha}} R_f^2 \Gamma_{target}^{2/\alpha} K_\alpha} \tag{24}$$

Therefore, $\bar{\lambda}_{FBS} = \min(\bar{\lambda}_{FBS,MUE}, \bar{\lambda}_{FBS,FUE})$ depicts the maximum density of FBS. In terms of the system bandwidth of N, FBS density is $\bar{\lambda}_{FB}$, and the achievable capacity in the downlink is depicted in (25).

$$C^{coch} = N\left(1+\bar{\lambda}_{FBS}\left|H\right|\right)\log_2(1+\Gamma_{target}) \tag{25}$$

Therefore, two key factors restricting the capacity in the downlink for the co-channel frequency allocation are RB resources and the density of FBS. The capacity increases with the increase of RB as depicted in Figure 2.7. And the maximum density exists which is mainly determined by MUE's tolerance to the co-channel interference.

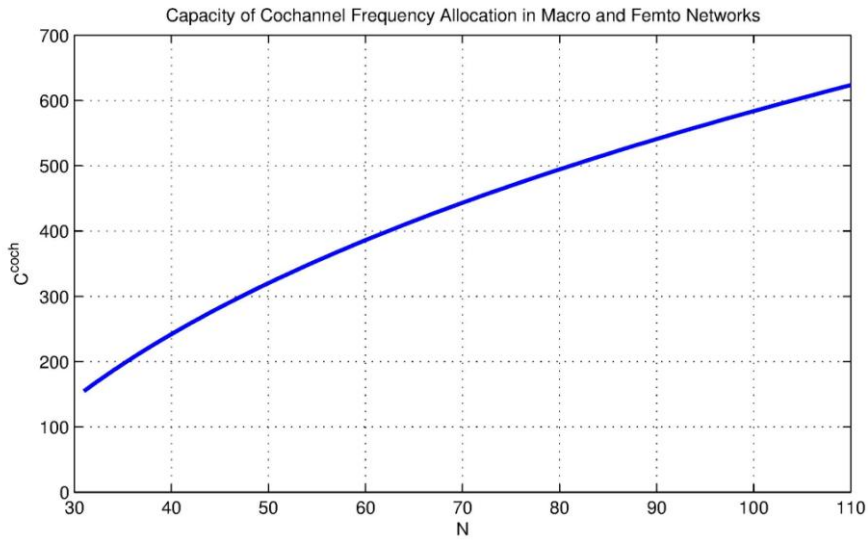

Figure 2.7 *System capacity in co-channel deployment for different* N *. SOURCE: Reproduced with permission from [29]. Copyright 2015 Springer International Publishing.*

2.2.4 Hybrid Frequency Allocation Scheme

Based on the analysis of orthogonal and co-channel frequency allocation schemes, the FBS density λ_{FBS} and the optimal RB resource ratio ρ will affect the capacity of hierarchical networks. However, the self-deployment and uncertainty of switch-on and switch-off features of FBS in practice are key challenges. Besides, the time delay of information exchange among hierarchical networks via a third party backhaul is another big problem unsolved. Therefore, it is difficult to make an optimal resource allocation scheme based on the FBS density in a practical scenario. Moreover, the co-channel frequency allocation scheme can provide an efficient spectrum utilization solution, but it inevitably introduces the strong co-channel interference which will decrease the system capacity.

Therefore, a dynamic hybrid frequency allocation scheme is proposed to increase the capacity, by taking into account the advantages of both orthogonal and co-channel frequency allocation schemes. The coverage of MBS is divided into inner and outer circle regions as shown in Figure 2.8. In the inner circle region, the FBS applies the orthogonal frequency allocation scheme. In the outer circle region, the FBS applies the orthogonal frequency allocation scheme when it is within the threshold radius R_{th} of MUE and applies the co-channel frequency allocation scheme when it is outside the threshold radius R_{th}. Thus, the hybrid frequency allocation scheme is described and analyzed in detail below, which can improve the capacity by increasing the density of FBS and the frequency reuse.

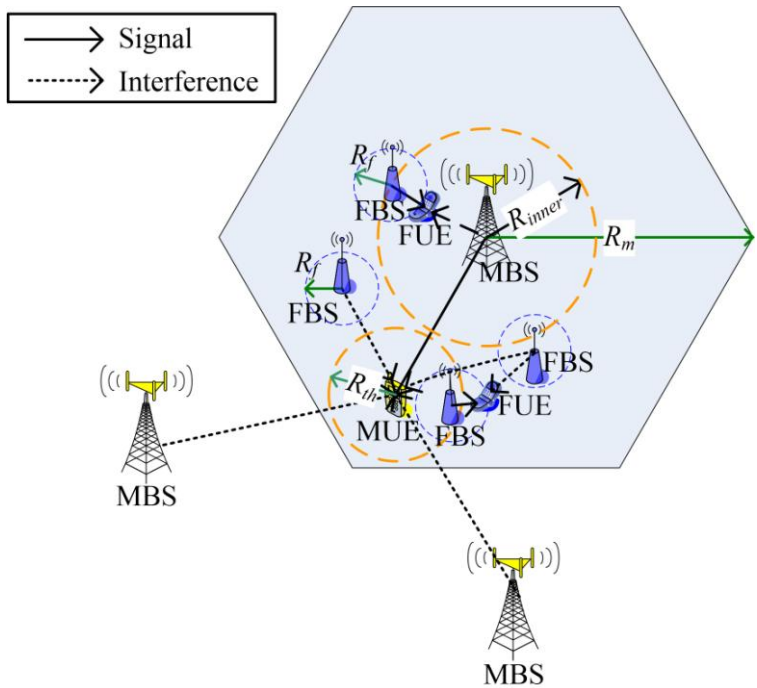

Figure 2.8 *Scenario of hybrid frequency allocation scheme. SOURCE: Reproduced with permission from [29]. Copyright 2015 Springer International Publishing.*

1) Capacity analysis of the inner circle region

To simplify the theoretical analysis and mathematical calculations, it is assumed that FUE will suffer from the strong co-channel interference from the serving MBS_0 and the interference from neighboring MBS_k $(k=1,2,...,6)$ is ignored. SINR of the FUE is denoted by $SINR_{f,inner}^{hybrid}$ in (26).

$$SINR_{f,inner}^{hybrid}\left(d_f\right)=\frac{G_f P_f d_f^{-\alpha}}{N_0+G_m P_m d_m^{-\alpha}} \tag{26}$$

d_f represents the distance between FBS and FUE, and d_m represents the distance between MBS and FUE. To simplify the analysis, the effect of channel gain from G_f and G_m to $SINR_{f,inner}^{hybrid}$ is ignored. When FUE is located at the edge of FBS as depicted by $d_f=R_f$, $SINR_{f,inner}^{hybrid}$ is denoted in (27).

$$SINR_{f,inner}^{hybrid}\left(R_f\right)=\frac{P_f R_f^{-\alpha}}{N_0+P_m d_m^{-\alpha}}=\Gamma_{target} \tag{27}$$

When $\alpha=4$ and $P_f R_f^{-\alpha}-N_0\Gamma_{target}>0$, the radius of FBS R_f should satisfy $R_f<\left(P_f/N_0\Gamma_{target}\right)^{1/4}=4.27\times10^2 m$. The radius R_{inner} of the inner cell region is depicted in (28).

$$R_{inner}=d_m+R_f=R_f+\left(\frac{\Gamma_{target}P_m}{P_f R_f^{-\alpha}-N_0\Gamma_{target}}\right)^{1/\alpha} \tag{28}$$

When R_f is small and the effect of the background noise to R_{inner} can be ignored, the R_{inner} is simplified as $R_{inner}\le R_f[1+(\Gamma_{target}P_m/P_f)^{1/4}]=5.95R_f\le R_m$.

Furthermore, the total number of RB is N and $(1-\rho)N$ is assigned to FBS. Considering the SINR of MUE at the cell edge $d_m = R_{inner}$ with the outage probability constraint ε, the R_{inner} is depicted in (29)-(30).

$$P\left(SINR_m^{hybrid}\left(R_{inner}\right) = G_m P_m R_{inner}^{-\alpha} / N_0 \geq \Gamma_{target}\right) \geq 1-\varepsilon \tag{29}$$

$$R_{inner} \leq \left[-\ln(1-\varepsilon)P_m / (N_0 \Gamma_{target})\right]^{1/\alpha} \tag{30}$$

Similarly, considering the SINR of FUE at the cell edge $d_m = R_{inner}$ with the outage probability constraint ε, the SINR of FUE is depicted in (31), where $s = \Gamma_{target} / [P_f R_f^{-\alpha}(1-\rho)N]$.

$$P\left(SINR_f^{hybrid}\left(R_f\right) = \frac{G_f P_f R_f^{-\alpha}}{N_0 + I_{f,f}^{hybrid} / (1-\rho)N} \geq \Gamma_{target}\right) = 1-\varepsilon \tag{31}$$

$$I_{f,f}^{hybrid} = \sum\nolimits_{Y_i \in \Phi_{FBS}^{p} \setminus \{Y_0\}, Y_i \leq 2R_{inner}} G_{Y_i} P_f \,\|Y_i\|^{-\alpha} \tag{32}$$

$$E[\exp(-sI_{f,f}^{\text{hybrid}})] = \exp[-\pi \bar{\lambda}_{\text{FBS}}^{R_{\text{inner}}} (sP_f)^{1/2} \tan^{-1}(4R_{\text{inner}}^2/(sP_f)^{1/2})] \tag{33}$$

By putting (32) and (33) into (31), the SINR of FUE is denoted in (34).

$$\begin{aligned} &P\left(SINR_f^{hybrid}\left(R_f\right) \geq \Gamma_{target}\right) \\ &= \exp[-N_0 \Gamma_{\text{target}} / (P_f R_f^{-\alpha})] \exp[-\pi \bar{\lambda}_{\text{FBS}}^{R_{\text{inner}}} (sP_f)^{1/2} \tan^{-1}(4R_{\text{inner}}^2/(sP_f)^{1/2})] = 1-\varepsilon \end{aligned} \tag{34}$$

Therefore, the density of FBS in the inner circle region is denoted by $\bar{\lambda}_{FBS}^{R_{inner}}$ in (35).

$$\bar{\lambda}_{FBS}^{R_{inner}} = \frac{-\ln(1-\varepsilon) - N_0 \Gamma_{target} / (P_f R_f^{-\alpha})}{\pi \sqrt{\Gamma_{target} R_f^{\alpha} / [(1-\rho)N]}\, tan^{-1}\left\{4R_{inner}^2 / \sqrt{\Gamma_{target} R_f^{\alpha} / [(1-\rho)N]}\right\}} \quad (35)$$

The capacity in the downlink within the inner circle region of the proposed hybrid frequency allocation scheme is depicted in (36), where $|H_{inner}| = \pi R_{inner}^2$.

$$C_{inner}^{hybrid} = N\left[\rho + (1-\rho)\bar{\lambda}_{FBS}^{R_{inner}} |H_{inner}|\right] \log_2(1+\Gamma_{target}) \quad (36)$$

When $N = 110$, $\rho = 0.28$, $\bar{\lambda}_{FBS}^{R_{inner}} = 1.10 \times 10^{-3}$, $R_{inner} = 59.5\text{m}$, the downlink capacity is $C_{inner}^{hybrid} = 2.0 \times 10^3 \text{bit/s}$.

2) Capacity analysis of the outer circle region

In the outer circle region of MBS, MUE will suffer from strong interferences from FBSs in the vicinity. Thus, FBS will apply the restricted co-channel frequency allocation scheme to be aware of the available RB resources in different locations by adding cognitive abilities. FBS will minimize the co-channel interference to MUE and increase the deployment density of small cells. Within the threshold radius R_{th} of MUE, the orthogonal frequency allocation scheme is applied to FBS to minimize the interference. Otherwise, the co-channel frequency allocation scheme is applied to FBS in the outer circle region of MBS.

In terms of the maximum outage probability ε, the SINR of MUE is depicted by $SINR_m^{hybrid}(d_m)$ in (37), which includes the interference from neighboring MBS and FBS outside the threshold radius of R_{th}.

$$SINR_m^{hybrid}\left(d_m\right)=\frac{G_m P_m d_m^{-\alpha}}{N_0+\frac{1}{N}\sum_{i=1}^{6} I_{m_i,m}+\frac{1}{N} I_{f,m}^{hybrid}} \tag{37}$$

$$\sum_{i=1}^{6} I_{m_i,m}=\sum_{i=1}^{6} G_{m_i} P_m \bar{d}_{m_i,m}^{-\alpha} \tag{38}$$

$$I_{f,m}^{hybrid}=\sum\nolimits_{Y_i\in\Phi_{FBS}^{p},\|Y_i\|\geq R_{th}} G_{Y_i} P_f \|Y_i\|^{-\alpha} \tag{39}$$

Where $I_{f,m}^{hybrid}$ depicts the interference from FBS outside the threshold radius R_{th} to MUE, $I_{m_i,m}$ represents the interference from neighboring MBS_i to MUE in MBS_0, $\bar{d}_{m_i,m}$ is the mean distance between MBS_i and MUE in MBS_0. When $\alpha=4$, the calculations can be simplified as denoted in (40).

$$E[\exp(-sI_{f,m}^{hybrid})]=\exp\{-\pi\bar{\lambda}_{FBS}^{R_{th}}(sP_f)^{1/2}[\pi/2-\tan^{-1}(R_{th}^2/(sP_f)^{1/2})]\} \tag{40}$$

In terms of the outage probability constraint ε, the SINR of MUE at the cell edge of MBS is depicted in (41).

$$P\left(SINR_m^{hybrid}\left(R_m\right)\geq\Gamma_{target}\right)\geq 1-\varepsilon \tag{41}$$

By putting (37) and (40) into (41), the SINR of MUE is denoted in (42), where only one strong interference from MBS_k is considered and $\bar{d}_{m_i,m}=R_m$. Furthermore, the density of FBS is denoted by $\bar{\lambda}_{FBS,MUE}^{R_{th}}$ in (43).

$$
\begin{aligned}
&P\left(SINR_m^{hybrid}\left(R_m\right)\geq\Gamma_{target}\right)\\
&=\frac{\exp(-\frac{\Gamma_{target}N_0}{P_mR_m^{-4}})}{1+\Gamma_{target}/N}\exp\left\{-\pi\bar{\lambda}_{FBS,MUE}^{R_{th}}R_m^2\sqrt{\frac{P_f\Gamma_{target}}{NP_m}}\left[\frac{\pi}{2}-\tan^{-1}\left(R_{th}^2R_m^{-2}/\sqrt{\frac{P_f\Gamma_{target}}{NP_m}}\right)\right]\right\} \qquad (42)\\
&\geq 1-\varepsilon
\end{aligned}
$$

$$
\bar{\lambda}_{FBS,MUE}^{R_{th}}=\frac{-\ln\left[\left(1-\varepsilon\right)\left(1+\frac{\Gamma_{target}}{N}\right)\right]-\frac{\Gamma_{target}N_0}{P_mR_m^{-4}}}{\pi R_m^2\sqrt{\frac{P_f\Gamma_{target}}{NP_m}}\left[\frac{\pi}{2}-\tan^{-1}\left(R_{th}^2R_m^{-2}/\sqrt{\frac{P_f\Gamma_{target}}{NP_m}}\right)\right]} \qquad (43)
$$

Thus, the capacity in the downlink for the outer circle region is depicted by C_{outer}^{hybrid} in (44).

$$
C_{outer}^{hybrid}=N\left(1+\bar{\lambda}_{FBS}^{outer}\left|H_{outer}\right|\right)\log_2(1+\Gamma_{target}) \qquad (44)
$$

Where $\left|H_{outer}\right|=\left|H\right|-\left|H_{inner}\right|=3\sqrt{3}/2\,R_m^2-\pi R_{inner}^2$ represents the outer circle region. And the total capacity in the downlink of inner and outer circle regions are denoted by C_{total}^{hybrid} in (45)-(46).

$$
C_{total}^{hybrid}=C_{inner}^{hybrid}+C_{outer}^{hybrid} \qquad (45)
$$

$$
C_{total}^{hybrid}=\left[\rho+\left(1-\rho\right)\bar{\lambda}_{FBS}^{R_{inner}}\left|H_{inner}\right|+1+\bar{\lambda}_{FBS}^{outer}\left|H_{outer}\right|\right]N\log_2(1+\Gamma_{target}) \qquad (46)
$$

In terms of different RB resources N and the threshold radius R_{th}, the capacity of hybrid frequency allocation scheme and co-channel frequency allocation scheme is compared as depicted in Figure 2.9. The capacity will increase with the increase of R_{th} in the outer circle region. By using the

orthogonal frequency allocation scheme for FBS within the threshold radius R_{th} of MUE in the outer circle region, the strong interference from FBS to MUE in the vicinity can be greatly minimized, which can improve the capacity in the downlink. Therefore, the proposed hybrid frequency allocation scheme can effectively minimize the cross-tier interference in hierarchical networks. When $N=110$, $\rho=0.28$, $R_{inner}=59.5\text{m}$, $R_{th}=50\text{m}$, $\bar{\lambda}_{FBS}^{R_{inner}}=1.10\times10^{-3}$, $\bar{\lambda}_{FBS}^{R_{outer}}=8.73\times10^{-6}$, the theoretical maximum capacity can achieve $C_{total}^{hybrid}=3.45\times10^{3}\,\text{bit/s}$.

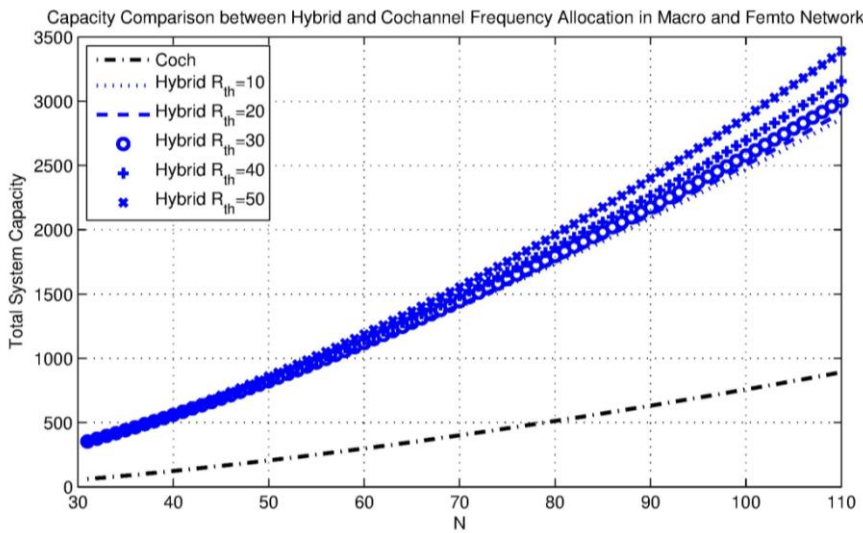

Figure 2.9 *Total capacity (hybrid vs. co-channel deployment). SOURCE: Reproduced with permission from [29]. Copyright 2015 Springer International Publishing.*

In summary, based on the analysis above, there are four key factors that will affect the capacity of hierarchical networks in the downlink. First, R_{inner} is used to identify the inner and outer cell regions, which is directly related to FBS coverage radius R_f . Second, the threshold radius R_{th} of MUE will affect the capacity which increases as R_{th} increases. Third, the RB resource N will

affect the capacity which will increase with the increase of N. Fourth, the network capacity will increase as the increase of $\bar{\lambda}_{FBS}$. Therefore, by optimal parameters design in the hybrid frequency allocation scheme, co-channel interference can be greatly minimized, which can increase the FBS deployment density and improve the network capacity.

2.3 Optimal Geographic Region Division Scheme for Small Cell Networks

According to 3GPP TR 36.814 [27], MBS and FBS are defined as different layers and the information exchange among them are limited due to the X2 interface and backhaul delay. Therefore, a feasible solution by using CPC technology is proposed to support the information exchange among MBS and FBS. By adding cognitive functions, the proposed solution applies the in-band CPC technology [22] to deliver the frequency occupancy information of MUE according to different geographic zones. Thereafter, the frequency self-deployment of FBS is carried out to improve the capacity of hierarchical networks.

According to the analysis above, the FBS deployment density $\bar{\lambda}_{FBS}$ is one of the key factors that will affect the capacity. By effectively utilizing the small coverage feature of FBS, the proposed optimal FBS deployment can improve the efficiency of frequency reuse to enhance the network capacity. As shown in Figure 2.10(a), by dividing the MBS coverage area into uniform square geographic regions, small cells can be aware of the frequency occupancy information of local zones via CPC technology. Therefore, FBS can utilize orthogonal frequency resources that is different from neighbour MUE to avoid co-channel interference and improve the network capacity. Considering the uncertainty and randomness of small cells coverage areas, the square geographic zones can not ideally match the contour of network coverage areas, which will lead to errors using different geographic region division schemes. Thus, the error

probability of different geographic region division schemes is theoretically analyzed. Then, the optimal region division scheme is proposed and achieved in different cases.

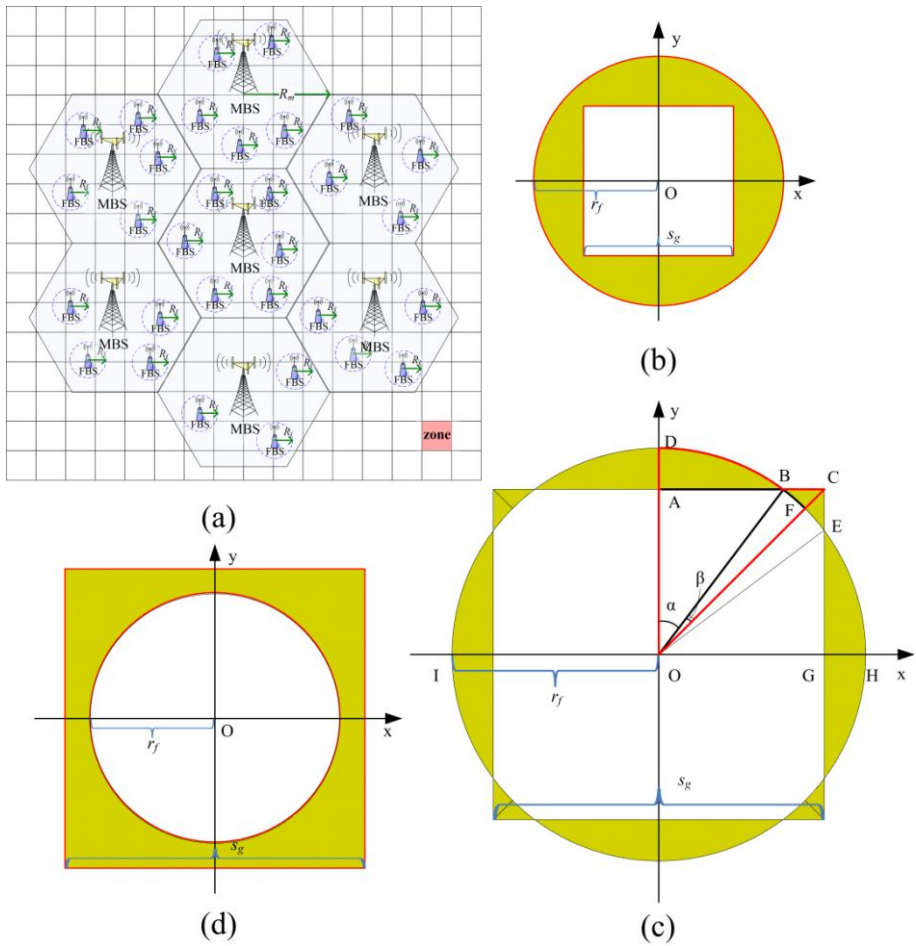

Figure 2.10 *Scenario of optimal zone division in different geographical regions. SOURCE: Reproduced with permission from [29]. Copyright 2015 Springer International Publishing.*

2.3.1 Error Probability of Different Geographic Region Division Schemes

The deployment of FBS is modeled as a uniform distribution with the density λ_{FBS}, and it is assumed that the coverage of FBS is a circle with a radius of r_f. The geographic zone is a square with a length of s_g and the error probability is denoted by p_{err} which is shown by the shadow area in Figure 2.10. To simplify the theoretical analysis, it is assumed that only one FBS overlaps with the square zone. Then, the error probability p_{err} is calculated with different r_f and s_g in three cases below.

Case1: As shown in Figure 2.10(b), when $0 < s_g \le \sqrt{2} r_f$, the normalized error probability p_{err1} using the geographic region division scheme is depicted in (47).

$$p_{err1} = (\pi r_f^2 - s_g^2) / \pi r_f^2 \tag{47}$$

Case2: As shown in Figure 2.10(c), when $\sqrt{2} r_f < s_g < 2 r_f$, the normalized error probability p_{err2} using the geographic region division scheme is depicted in (48), where $\angle AOB = \alpha = \arccos(s_g / 2r_f)$, $\angle BOC = \beta = \pi / 4 - \alpha$, $0 < \alpha, \beta < \pi / 4$. $S_{OBD}, S_{OBA}, S_{OCB}, S_{OFB}$ depict the triangle areas.

$$\begin{aligned} p_{err2} &= 8 / \pi r_f^2 [(S_{OBD} - S_{OBA}) + (S_{OCB} - S_{OFB})] \\ &= 8 / \pi r_f^2 \{(\alpha r_f^2 / 2 - \sqrt{4r_f^2 - s_g^2} s_g / 8) + [(s_g - \sqrt{4r_f^2 - s_g^2}) s_g / 8 - \beta r_f^2 / 2]\} \\ &= 1 / \pi r_f^2 [8 r_f^2 \arccos(s_g / 2r_f) - \pi r_f^2 + s_g^2 - 2 s_g \sqrt{4r_f^2 - s_g^2}] \end{aligned} \tag{48}$$

Case3: As shown in Figure 2.10(d), when $s_g \ge 2 r_f$, the normalized error probability p_{err3} using the geographic region division scheme is depicted in (49).

$$p_{err3} = (s_g^2 - \pi r_f^2) / \pi r_f^2 \tag{49}$$

The normalized error probability of dividing geographic region p_{err} is denoted in (50).

$$p_{err} = \begin{cases} \left(\pi r_f^2 - s_g^2\right) / \pi r_f^2 & when\ 0 < s_g \le \sqrt{2} r_f \\ 8 r_f^2 \arccos(\frac{s_g}{2r_f}) - \pi r_f^2 + s_g^2 - 2 s_g \sqrt{4 r_f^2 - s_g^2} / \pi r_f^2 & when\ \sqrt{2} r_f < s_g < 2 r_f \\ \left(s_g^2 - \pi r_f^2\right) / \pi r_f^2 & when\ s_g \ge 2 r_f \end{cases} \tag{50}$$

2.3.2 Optimal Geographic Region Division Scheme

The optimal geographic region division scheme is defined as an optimization problem that how to design an optimal square zone length s_g^{Opt} with the minimum error probability p_{err}, as denoted in (51).

$$s_g^{Opt} = \arg\min_{s_g} p_{err} \tag{51}$$

(1) When $0 < s_g \le \sqrt{2} r_f$, p_{err1} is a monotonically decreasing function as denoted in (52). The minimum error probability achieves $p_{err1}^{\min} = p_{err1}(\sqrt{2} r_f) = \pi - 2/\pi = 0.36$, when $s_g = \sqrt{2} r_f$.

$$dp_{err1} / ds_g = -2 s_g / (\pi r_f^2) < 0 \tag{52}$$

(2) When $\sqrt{2} r_f < s_g < 2 r_f$, by applying $s_g = 2 r_f \cos\alpha$ in (48), p_{err2} is depicted in (53), where $\gamma = \arcsin(2/\sqrt{5})$. When $\alpha = \pi/2 - \arcsin(2/\sqrt{5})$,

$s_g = 2r_f \cos\alpha = 1.79r_f$, the minimum error probability is $p_{err2}^{\min} = \left[3\pi - 8\arcsin(2/\sqrt{5})\right]/\pi = 0.18$.

$$p_{err2} = \frac{1}{\pi}\left[2 - \pi + 8\alpha + 2\sqrt{5}\cos(2\alpha + \gamma)\right], \tag{53}$$

(3) When $s_g \geq 2r_f$, p_{err3} is a monotonically increasing function as denoted in (54). The minimum error probability achieves $p_{err3}^{\min} = p_{err3}(2r_f) = (4-\pi)/\pi = 0.27$, when $s_g = 2r_f$.

$$dp_{err3}/ds_g = 2s_g/(\pi r_f^2) > 0 \tag{54}$$

Therefore, the minimum error probability using geographic region division scheme achieves $p_{err}^{\min} = \min(p_{err1}^{\min}, p_{err2}^{\min}, p_{err3}^{\min}) = p_{err2}^{\min} = 0.18$, when the optimal square zone length $s_g^{Opt} = \arg\min_{s_g} p_{err} = 1.79r_f$. In addition, under different geographic region division ratio s_g / r_f conditions, the trend of error probability p_{err} is depicted in Figure 2.11. Then, the minimum error probability achieves $p_{err}^{\min} = 0.18$ and the optimal square zone length is $s_g^{Opt} = 1.79r_f$.

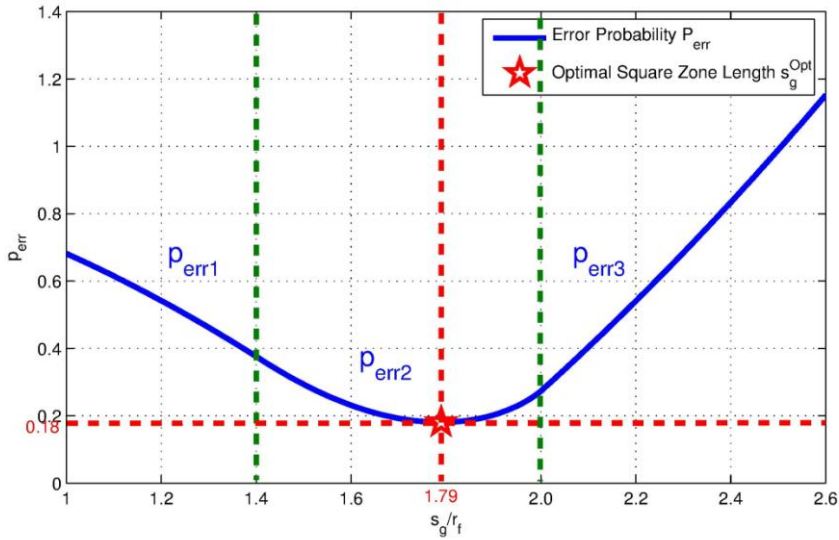

Figure 2.11 *Minimum error probability* p_{err} *and square zone length* s_g / τ_f *using the optimal geographic region division scheme. SOURCE: Reproduced with permission from [29]. Copyright 2015 Springer International Publishing.*

2.4 Self-deployment Procedure of Hybrid Frequency Allocation Scheme

In order to efficiently deliver the frequency occupancy information of MBS in different geographic zones, the in-band CPC technology is applied as a candidate solution in [22]. Therefore, the self-deployment procedure of FBS using hybrid frequency allocation scheme is shown in Figure 2.12.

Step 1: FBS starts up and works in the listening mode. And FBS receives the frequency occupancy information of MBS via the CPC channel and exchanges the self-deployment default parameters with the core network via backhaul links.

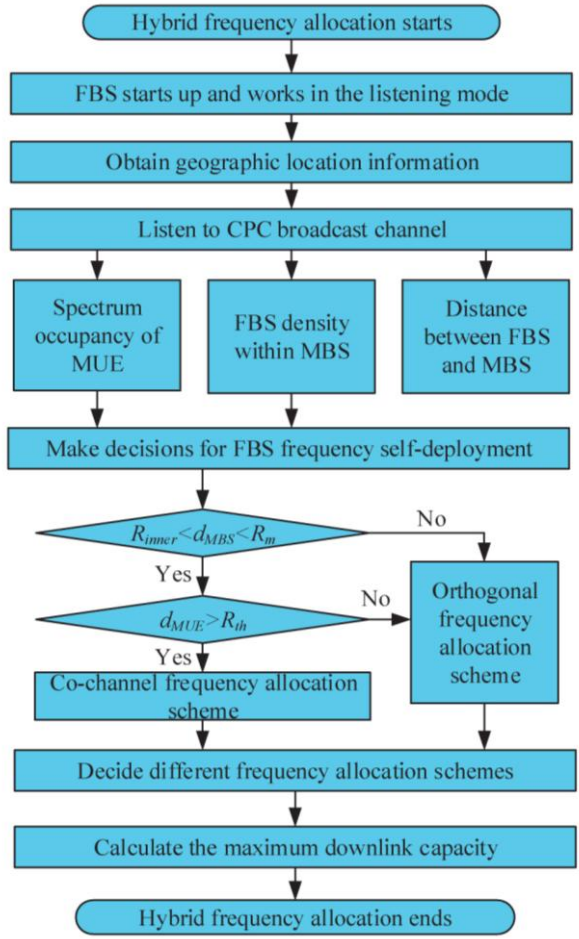

Figure 2.12 *Procedure of hybrid frequency allocation scheme. SOURCE: Reproduced with permission from [29]. Copyright 2015 Springer International Publishing.*

Step 2: FBS monitors the CPC channel and depicts key parameters of heterogeneous networks, such as the frequency occupancy information of MUE within the vicinity of FBS, the density of FBS, the received signal strength of MBS to estimate the distance between FBS and MBS.

Step 3: FBS makes spectrum self-deployment decisions based on the calculation of R_{inner} and R_{th}. By comparing the distance of d_{MBS} to R_{inner}, FBS

can decide whether it belongs to the inner circle region or the outer circle region. Then, FBS makes a decision on applying different frequency allocation schemes, such as orthogonal, co-channel and hybrid frequency allocation schemes, based on the distance between d_{MUE} and R_{th}.

Step 4: The maximum capacity of heterogeneous network is calculated and the procedure of hybrid frequency allocation scheme ends.

2.5 Results and Performance Analyses

In this part, numerical results of SINR and capacity of FBS and MBS are described by applying the proposed hybrid frequency allocation scheme. A typical scenario is depicted in Figure 2.13, which includes seven MBSs and the proposed outer and inner circle regions. Key parameters in this typical simulation scenario are denoted in Table 2.1 [27]. Simulation results of various SINR and capacity values with different FBS densities and distances between MBS and FBS are analyzed below by using the proposed hybrid frequency allocation scheme.

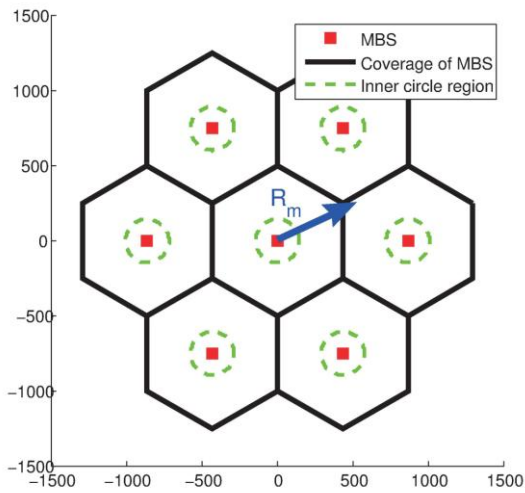

Figure 2.13 *Simulation scenario. SOURCE: Reproduced with permission from [29]. Copyright 2015 Springer International Publishing.*

Table 2.1 *Simulation parameters. SOURCE: Reproduced with permission from [29]. Copyright 2015 Springer International Publishing.*

Parameter	Value
Transmit Power of MBS P_m (W)	20
Transmit Power of FBS P_f (W)	0.1
System Bandwidth BW (MHz)	20
RB Number N	110
Path Loss α	4
Target $SINR$ (dB)	3
Maximum Outage Probability ϵ	0.1
Coverage Radius of MBS R_m (m)	500
Coverage Radius of FBS R_f (m)	10
Background Noise Power N_0 (W)	10^{-12}
Inner Circle Region Radius R_{inner} (m)	59.5
Threshold Radius R_{th} (m)	10, 20, 30, 40, 50

2.5.1 SINR Analysis of Hybrid Frequency Allocation Scheme

The SINR distribution of MUE in different locations in the hybrid frequency allocation scheme is shown in Figure 2.14, where the warmer color denotes a much higher SINR value. MUE in the outer circle region will suffer the strong interference from neighbour MBSs and FBSs outside a distance of R_{th}, which will greatly increase with the surge of FBS density λ_{FBS} from λ_1 to λ_3. Furthermore, the SINR distribution of MUE is also depicted in Figure 2.15 which demonstrates the effect of the distance between MUE and MBS to SINR values. Two curves of the orthogonal frequency allocation scheme and the target SINR value are also plotted in 200 m away from MBS, which denotes that the orthogonal frequency allocation scheme is applied to FBS within a distance of

R_{th} of MUE. With the increase of FBS density λ_{FBS}, the SINR value of MUE will decrease extensively which denotes that MUE suffers from the strong interference from neighbour FBSs outside a distance of R_{th}. Therefore, MUE at the edge of MBS can dynamically increase the threshold radius R_{th} to decrease the co-channel interference from densely deployed FBSs.

Moreover, the SINR distribution of FUE is shown in Figure 2.16 with different FBS density values. With the increase of FBS, the SINR of FUE within FBS's coverage increases. But when the density of FBS is extensively large, the SINR of FUE will decrease due to the strong interference from neighbour FBSs around the FUE. Thus, the SINR distribution of FUE is also depicted in Figure 2.17 which demonstrates the effect of the distance between FUE and MBS to SINR values. Two curves of the orthogonal frequency allocation scheme and the target SINR value are also plotted in Figure 2.17. The SINR value of FUE achieves several small peaks at the distance around $200\,\mathrm{m}$ and $300\,\mathrm{m}$ away from MBS, which denotes that the orthogonal frequency allocation scheme is applied to neighbour FBSs to decrease co-channel interferences. Furthermore, the appropriate increase of R_{th} can also decrease the co-channel interference to FUE from neighbour FBSs, especially when the FBS density λ_{FBS} is large.

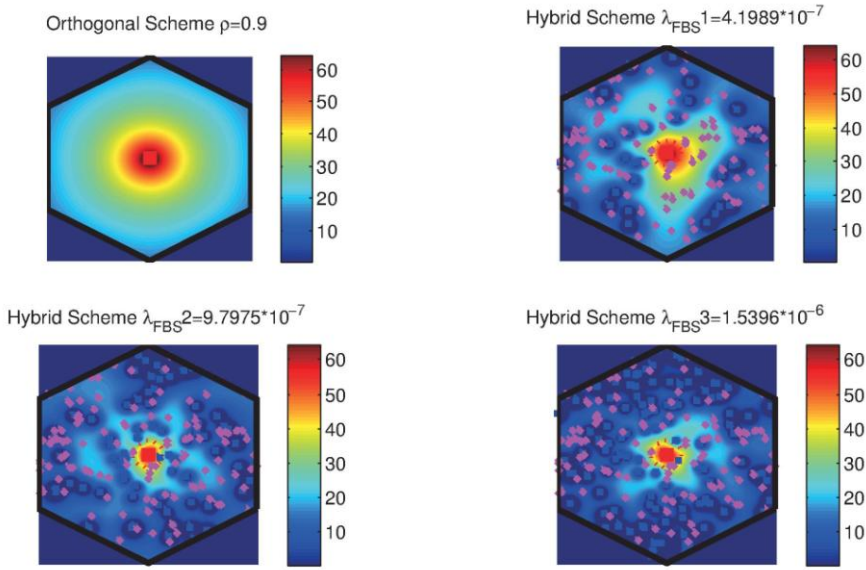

Figure 2.14 *SINR of MUE with different FBS density* λ_{FBS}. *SOURCE: Reproduced with permission from [29]. Copyright 2015 Springer International Publishing.*

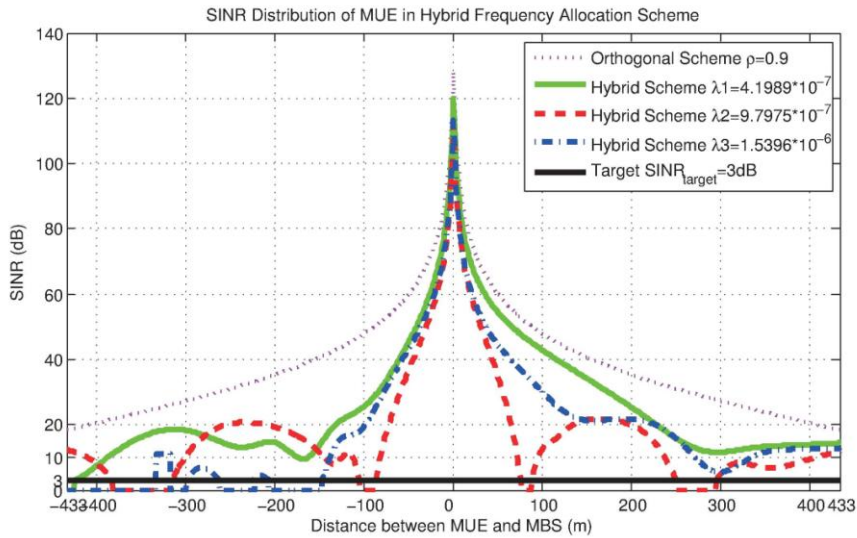

Figure 2.15 *SINR distribution of MUE with different distances between MUE and MBS. SOURCE: Reproduced with permission from [29]. Copyright 2015 Springer International Publishing.*

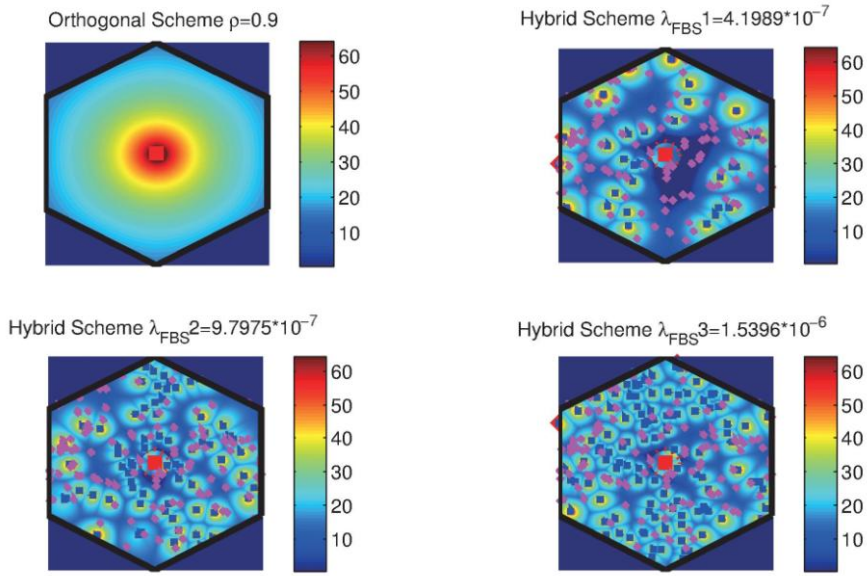

Figure 2.16 *SINR of FUE with different FBS density* λ_{FBS} *. SOURCE: Reproduced with permission from [29]. Copyright 2015 Springer International Publishing.*

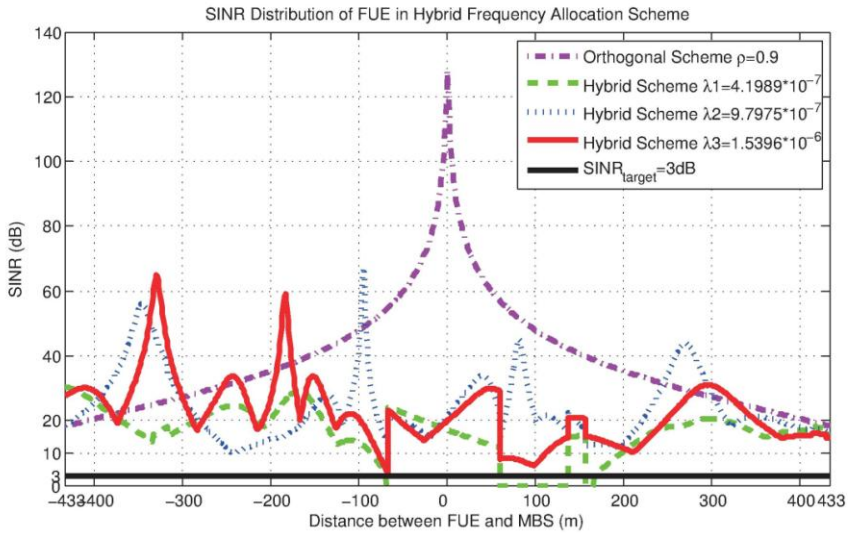

Figure 2.17 *SINR distribution of FUE with different distances between FUE and MBS. SOURCE: Reproduced with permission from [29]. Copyright 2015 Springer International Publishing.*

2.5.2 Capacity Analysis of Hybrid Frequency Allocation Scheme

As shown in Figure 2.18, the capacity of MBS increases with the increase of MUE density. Due to the co-channel interference from densely deployed neighbour FBSs, the capacity of MBS decreases with the increase of FBS density λ_{FBS}. Moreover, the total capacity C^{hybrid} will increase with the surge of FBS density λ_{FBS} as shown in Figure 2.19, which depicts that the densely deployed FBSs can increase the total capacity with appropriate R_{th} by minimizing the co-channel interference. And the total capacity will also increase with the increase of MUE density. Moreover, the co-channel interference from neighbour FBS to MUE can be minimized and the capacity of MBS and FBS will also increase with the increase of R_{th} in Figure 2.20 and Figure 2.21.

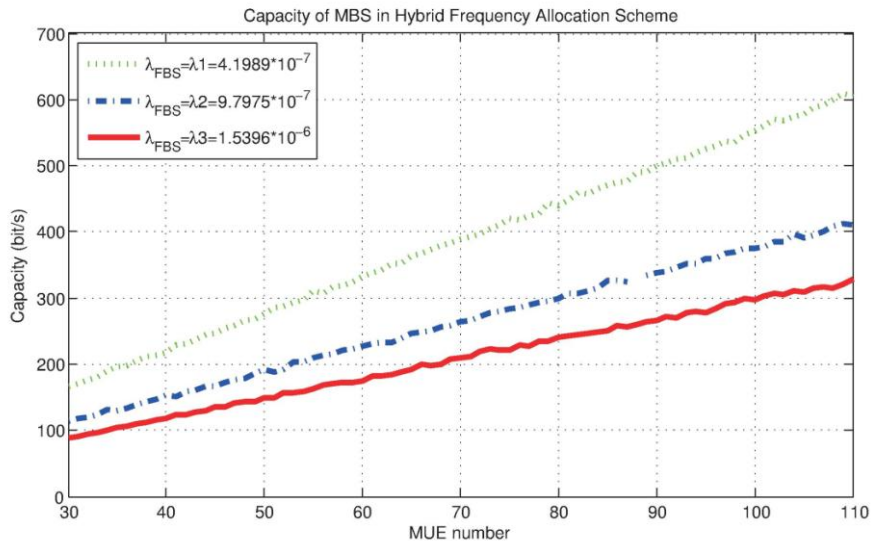

Figure 2.18 *Capacity of MBS with different FBS density and MUE density. SOURCE: Reproduced with permission from [29]. Copyright 2015 Springer International Publishing.*

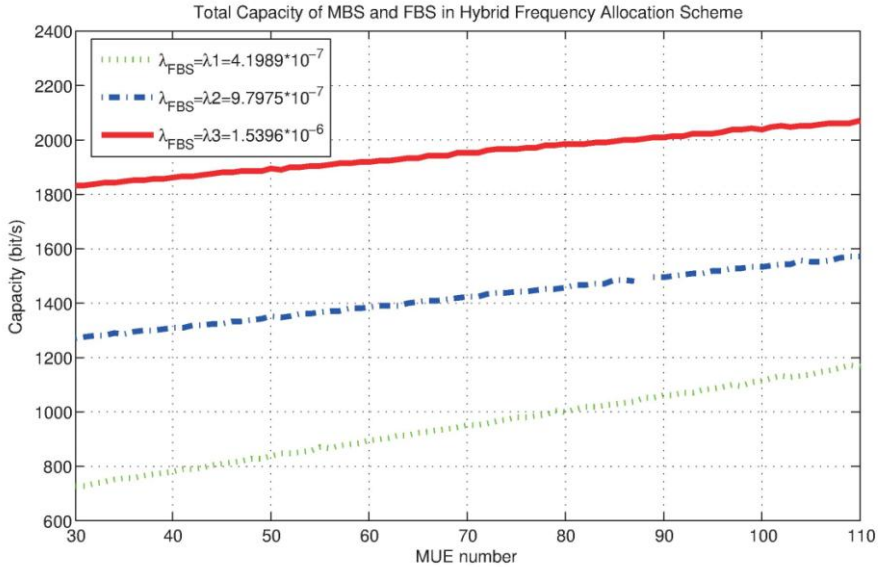

Figure 2.19 *Total capacity of MBS and FBS with different FBS density and MUE density. SOURCE: Reproduced with permission from [29]. Copyright 2015 Springer International Publishing.*

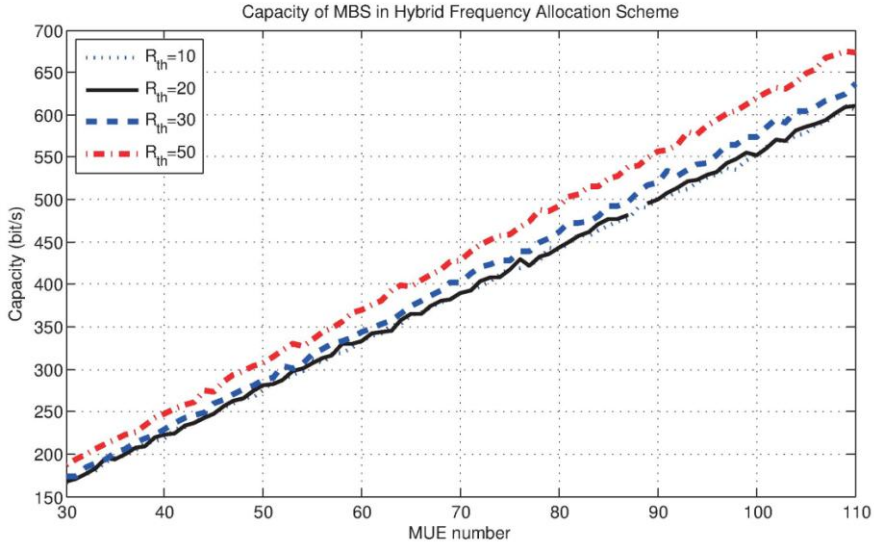

Figure 2.20 *Capacity of MBS with different* R_{th} *. SOURCE: Reproduced with permission from [29]. Copyright 2015 Springer International Publishing.*

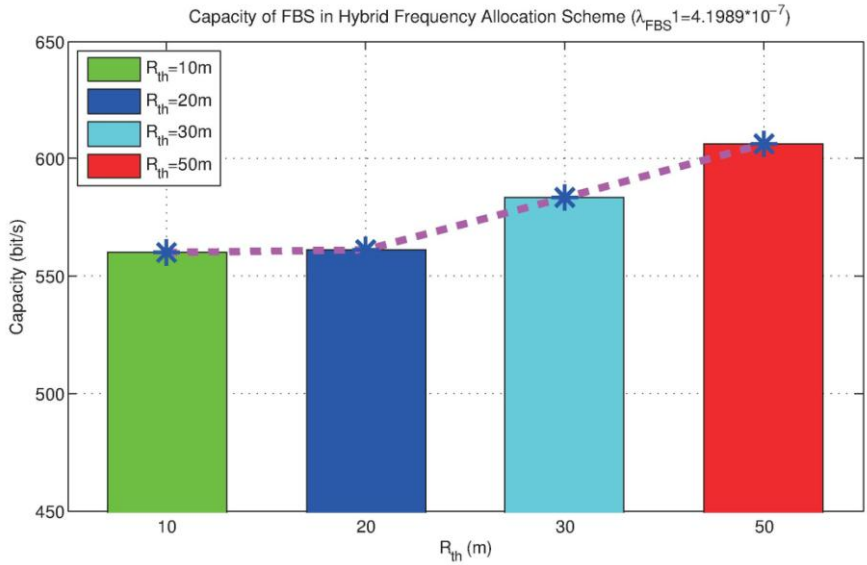

Figure 2.21 *Capacity of FBS with different* R_{th} *. SOURCE: Reproduced with permission from [29]. Copyright 2015 Springer International Publishing.*

2.6 Concluding Remarks

To increase the capacity of hierarchical networks, a hybrid frequency allocation scheme for densely deployed small cells is proposed. Based on the theoretical modeling and mathematical analysis, three frequency allocation schemes are proposed and key parameters affecting the capacity are defined and proved with closed-form solutions in different scenarios. Both the outer and inner circle regions are proposed to minimize the co-channel interference to MUE from neighbour FBSs. Then, the optimal geographic region division scheme is proposed with the optimal square zone length solutions, which can improve the information delivery among small cells. Furthermore, the self-deployment procedure of proposed hybrid frequency allocation scheme is designed and described in detail. Finally, numerical results are presented and analyzed to verify

the capacity improvement of the proposed scheme by considering the density of FBS, co-channel interference and the spatial separation among small cells.

Reference

[1] G. Mansfield. "Femtocells in the US market-business drivers and consumer propositions", *in Proc. Femtocells Europe*, ATT, London, 2008.

[2] J. Zhang, G. de la Roche, *Femtocells: technologies and deployment*, John Wiley & Sons, 2010.

[3] J. Cullen, "Radioframe presentation", *Femtocell Europe*, London, 2008.

[4] Cisco VNI forecast white paper, Cisco visual networking index: global mobile data traffic forecast update, pp. 2013-2018, 2014.

[5] W. Webb, *Wireless communications: the future*, John Wiley & Sons, 2007.

[6] V. Chandrasekhar, J. G. Andrews and A. Gatherer, "Femtocell networks: a survey", *IEEE Commun. Mag.*, vol. 46, no. 9, pp. 59-67, Sept. 2008.

[7] J. G. Andrews, H. Claussen, M. Dohler, S. Rangan and M. C. Reed, "Femtocells: past, present, and future", *IEEE J. Sel. Areas Commun.*, vol. 30, no. 3, pp. 497-508, Apr. 2012.

[8] P. Xia, V. Chandrasekhar and J. G. Andrews, "Femtocell access control in the TDMA/OFDMA uplink", *in Proc. IEEE Globecom*, Miami, FL, pp. 1-5. 2010.

[9] H. Elsawy, E. Hossain and D. I. Kim, "HetNets with cognitive small cells: user offloading and distributed channel access techniques", *IEEE Commun. Mag.*, vol. 51, no. 6, pp. 28-36, Jun. 2013.

[10] D. Mavrakis, *Small cell market status*, Informa Telecoms & Media, 2013.

[11] P. Xia, V. Chandrasekhar and J. G. Andrews, "Open vs. closed access femtocells in the uplink", *IEEE Trans. Wireless Commun.*, vol. 9, no. 12, pp. 3798-3809, Dec. 2010.

[12] V. Chandrasekhar and J. G. Andrews, "Spectrum allocation in tiered cellular networks", *IEEE Trans. Commun.*, vol. 57, no. 10, pp. 3059-3068, Oct. 2009.

[13] W. C. Cheung, T. Q. S. Quek and M. Kountouris, "Throughput optimization, spectrum allocation, and access control in two-tier femtocell networks", *IEEE J. Sel. Areas Commun.*, vol. 30, no. 3, pp. 561-574, Apr. 2012.

[14] I. Guvenc, M. R. Jeong, F. Watanabe and H. Inamura, "A hybrid frequency assignment for femtocells and coverage area analysis for co-channel operation", *IEEE Commun. Lett.*, vol. 12, no. 12, pp. 880-882, Dec. 2008.

[15] A. Galindo-Serrano, L. Giupponi and M. Dohler, "Cognition and docition in OFDMA-based femtocell networks", *in Proc. IEEE Globecom*, Miami, FL, Dec. 6-10, 2010.

[16] V. Chandrasekhar and J. G. Andrews, "Uplink capacity and interference avoidance for two-tier femtocell networks", *IEEE Trans. Wireless Commun.*, vol. 8, no. 7, pp. 3498-3509, Jul. 2009.

[17] D. Lopez-Perez, A. Valcarce, G. de la Roche and J. Zhang, "OFDMA femtocells: a roadmap on interference avoidance", *IEEE Commun. Mag.*, vol. 47, no. 9, pp. 41-48, Sept. 2009.

[18] D. Lopez-Perez, A Ladanyi, A. Juttner and J. Zhang, "OFDMA femtocells: a self-organizing approach for frequency assignment", *in Proc. IEEE PIMRC*, Tokyo, Japan, pp. 2202-2207, Sept. 2009.

[19] S. Y. Lien, C. C. Tseng, K. C. Chen and C. W. Su, "Cognitive radio resource management for QoS guarantees in autonomous femtocell networks", *in Proc. IEEE ICC*, Cape Town, pp. 1-6, May 2010.

[20] H. ElSawy and E. Hossain, "Two-tier HetNets with cognitive femtocells: downlink performance modeling and analysis in a multichannel environment", *IEEE Trans. Mob. Comput.*, vol. 13, no. 3, pp. 649-663, Mar. 2014.

[21] C. H. M. de Lima, M. Bennis and M. Latva-aho, "Coordination mechanisms for self-organizing femtocells in two-tier coexistence scenarios", *IEEE*

Trans. Wireless Commun., vol. 11, no. 6, pp. 2212-2223, Jun. 2012.

[22] Q. Zhang, Z. Feng, G. Zhang, "Efficient mesh division and differential information coding schemes in broadcast cognitive pilot channel", *Wireless Pers. Commun.*, vol. 63, no. 2, pp. 363-392, Mar. 2012.

[23] K. Nolte, A. Kaloxylos, K. Tsagkaris, "The E3 architecture: enabling future cellular networks with cognitive and self-x capabilities", *Int. J. Network Management*, vol. 21, no. 5, Sept. 2011.

[24] S. M. Cheng, W. C. Ao and K. C. Chen, "Downlink capacity of two-tier cognitive femto networks", *in Proc. IEEE PIMRC*, Istanbul, pp. 1303-1308, Sept. 2010.

[25] J. Kingman, *Poisson processes*, Oxford University Press, 1993.

[26] Poisson process website, http://en.wikipedia.org/wiki/Poisson_distribution\#2-dimensional_Poisson_process.

[27] "3GPP TSG RAN (E-UTRA): Further advancements for E-UTRA physical layer aspects (Release 9)", 3GPP TR 36.814 V9.0.0, 3rd Generation Partnership Project (3GPP), 2010.

[28] F. Baccelli, B. Blaszczyszyn and P. Muhlethaler, "An aloha protocol for multihop mobile wireless networks", *IEEE Trans. Inf. Theory*, vol. 52, no. 2, pp. 421-436, Feb. 2006.

[29] Q. Zhang, Z. Feng, Y. Zhang and T. Yang, "Hybrid frequency allocation scheme for capacity improvement in densely deployed small cells", *EURASIP J. Wireless Comm. and Networking*, 2015 (62), pp. 1-19, Jun. 2015.